Experimentally validated numerical analysis of aerostructures incorporating shape memory alloys

Darren Hartl, Jesse Mooney, Dimitris Lagoudas, James Mabe, Frederick Calkins

Darren J. Hartl, Jesse T. Mooney, Dimitris C. Lagoudas, James H. Mabe, Frederick T. Calkins, "Experimentally validated numerical analysis of aerostructures incorporating shape memory alloys," Proc. SPIE 6929, Behavior and Mechanics of Multifunctional and Composite Materials 2008, 692913 (3 April 2008); doi: 10.1117/12.776356

SPIE.

Event: SPIE Smart Structures and Materials + Nondestructive Evaluation and Health Monitoring, 2008, San Diego, California, United States

Experimentally Validated Numerical Analysis of Aerostructures Incorporating Shape Memory Alloys

Darren J. Hartl, Jesse T. Mooney and Dimitris C. Lagoudas
Texas A&M University, College Station, TX, U.S.A.

James H. Mabe and Frederick T. Calkins
The Boeing Company, Seattle, WA, U.S.A.

ABSTRACT

As the use of active structures continues to become more commercially viable, the need for accurate numerical modeling has gained importance. A current example of such a smart structure includes the variable geometry chevron. Future applications are also being designed, including a variable area jet engine nozzles and a torque tube actuators for rotor blades. This work concentrates on the FEA modeling of the Ni60Ti40 (wt %) SMA used in these applications and subsequent experimental validation. The constitutive model employed for the SMA material accounts for the full thermomechanical response and also accounts for such aspects as variable maximum transformation strain and smooth material hardening during transition. Model calibration is performed via uniaxial material testing. An overview of the model and material properties is presented followed by a discussion of the analysis results for the complex aerospace actuation applications. Comparisons to experimental validation of the overall system response are made.

Keywords: shape memory alloys, SMA, chevron, active materials, smart structures

1. INTRODUCTION

Shape memory alloys continue to become increasingly attractive as possible design solutions for engineers facing new technical challenges. Because of their unique properties, especially their potential for implementation as material actuators, Shape Memory Alloys (SMAs) have been proposed for use in a number of aerospace applications.[1] One of the earliest is as couplings for hydraulic lines in F-14 fighter jets in 1970's.[2] In the 1990's, researchers were interested in applying the unique properties of SMAs to more active structures. The DARPA "Smart Wing" project[3,4] examined the use of shape memory alloys and other active materials to warp and deform aircraft wings from within. Likewise, the SAMPSON project probed the feasibility of tailoring jet engine intake and exhaust geometry using SMA elements in various forms.[5] Similar work was performed by various entities, including the wing-warping work of Strelec et. al.[6] Regarding helicopter applications, SMAs have provided engineering solutions for actuators placed within confined geometric spaces and undergoing high dynamic loads.[7,8]

Currently, research is being performed on a completely new set of aerospace actuation applications. One example is the Variable Geometry Chevron (VGC).[9] The reduction of community noise at airports generated during aircraft take-off has become a major research goal. Serrated aerodynamic devices along the trailing edge of a jet engine primary and secondary exhaust nozzle, known as chevrons, have been shown to greatly reduce jet noise by encouraging advantageous mixing of the streams. Engineers at The Boeing Company have applied SMA materials to this problem of jet engine noise. Active chevrons, utilizing SMA components, have been developed and tested to create maximum deflection during takeoff and landing while minimizing deflection into the flow during the remainder of flight, increasing efficiency. Boeing has flight tested one system which includes active SMA beams encased in a composite structure with a complex 3-D configuration.[10] NASA researchers have also addressed the problem of active noise reduction by fabricating composite chevrons which include SMA tensile strips located at an offset from the chevron centroid. Such strips, when thermally transformed, induce bending of the total structure.[11] Motivated by the success of the VGC and other smart structure programs, new

Further author information: (Send correspondence to D.C.L.)
E-mail: lagoudas@aero.tamu.edu, Telephone: 1 979 845 9409

Behavior and Mechanics of Multifunctional and Composite Materials 2008,
edited by Marcelo J. Dapino, Zoubeida Ounaies, Proc. of SPIE Vol. 6929, 692913, (2008)
0277-786X/08/$18 · doi: 10.1117/12.776356

applications have also been proposed. These include a new SMA-driven variable geometry nozzle to optimize jet engine performance and various SMA torque tube applications for rotor twisting and control surface operation. The data presented in this work, while obtained in the context of the VGC development, will be used as the design of these future applications.

Expanded interest in SMA applications of all types has led to a greater need for more powerful design and analysis tools. This in turn has led to an interest in more accurate 3-D constitutive models, and these models must be motivated and calibrated using carefully obtained material characterization data. This work addresses such a characterization effort and focuses on a particular alloy composition. The VGC problem was modeled using a numerical implementation of the "unified model".[12,13] This specific model requires a particular set of material properties to be determined.[14] These include elastic properties unique to each phase, properties which describe transformation criteria (i.e., parameterized description of the phase diagram), and properties which describe the generation of recoverable transformation strain. Each of these property types will be investigated for a particular NiTi-based alloy in the current work. Although the most popular and prolific shape memory alloy system is near-equiatomic NiTi (Nitinol), the chevrons are actuated by active SMA components composed of $Ni_{60}Ti_{40}$ (wt%) or $Ni_{55}Ti_{45}$ (at%) (hereafter referred to as "Ni60Ti").

The organization of this paper is as follows: Sect. 2 describes the numerical tools utilized for the subject analysis of this work and Sect. 3 provides an overview of the material properties assigned to the Ni60Ti material based on thermomechanical characterization. The structural analyses setups and predictions and their comparisons with experimental data are discussed in Sect. 4 while the conclusions are summarized in Sect. 5.

2. THE UNIFIED SMA MODEL AS A NUMERICAL ANALYSIS TOOL

For this structural modeling effort, the baseline constitutive model chosen to predict the thermomechanical response of an SMA structural element was the unified model proposed by Lagoudas and coworkers[12] as implemented in an ABAQUS/Standard environment using return mapping algorithms.[13,15] However, due to particular characteristics of the material response as observed during experimental thermomechanical loading, particular assumptions within the model had to be reassessed. While derivations and discussions of the original form can be found in the literature,[12] and will not be addressed here, the new additions necessitated by the material behavior will be briefly discussed. In particular, two material effects requiring consideration but not explicitly addressed in the original model implementation were: *i.* the variation of maximum transformation strain with applied stress; and *ii.* the smoothness of the material response.

2.1. Implementation of Generalized Evolution Equation

In many SMA compositions, especially near equiatomic NiTi, training of the material will lead to two-way shape memory effect (TWSME). As a result, the maximum transformation strain generated during forward transformation can be independent of applied stress. In its originally implemented form, the unified model was intended to capture the response of these materials in particular that exhibit TWSME. However, the Ni60Ti of material of interest, though trained, did not seem to exhibit TWSME but rather generated increasing forward transformation strain with increasing applied stress. Therefore it was necessary to add this capability to the UMAT implementation. This effect enters into the evolution equation for the transformation or actuation strain $\boldsymbol{\varepsilon}^t$ which has the following form in the unified model:[12]

$$\dot{\boldsymbol{\varepsilon}}^t = \boldsymbol{\Lambda}\dot{\xi} \tag{2.1}$$

where $\boldsymbol{\Lambda}$ has been modified to take the current form[16]

$$\boldsymbol{\Lambda} = \begin{cases} \frac{3}{2}H^{cur}(\sigma)\frac{\boldsymbol{\sigma}'}{\overline{\boldsymbol{\sigma}}} & ; \quad \dot{\xi} > 0 \\ \frac{\varepsilon^{t-r}}{\xi^r} & ; \quad \dot{\xi} < 0 \end{cases} \tag{2.2}$$

This introduces the magnitude of the transformation strain generated during full forward transformation (i.e., maximum transformation strain) as a function of the applied stress level, $H^{cur}(\sigma)$. Here $\boldsymbol{\sigma}'$ is the stress deviator,

$\overline{\boldsymbol{\sigma}}$ is the effective stress, ε^{t-r} is the transformation strain at the reversal of phase transformation, and ξ^r is the martensitic volume fraction at the reversal of phase transformation. $H^{cur}(\sigma)$ is a function with a form motivated by the experimental results. This will be further discussed in Sect. 3.

2.2. Implementation of a "Smooth" Hardening Function

An additional alteration to the UMAT implementation of the unified model is related to the material hardening during transformation. Even by its name, the "unified" model was postulated to combine three distinct proposed forms for the hardening functions: the exponential, polynomial, and cosine forms. These were proposed by Tanaka,[17] Boyd and Lagoudas,[18] and Liang and Rogers,[19] respectively. This work includes the implementation of a new hardening function as proposed by Machado et al.[20] This hardening function was developed in the course of studying the non-linear dynamics of pseudoelastic SMAs, during which it was noted that a smooth function with smooth first derivatives would stabilize the numerical solution process and, more importantly, better capture the constitutive response of stabilized SMA actuation. To simplify implementation, the new function was developed within the framework of the existing unified model and thus solution methods such as the return mapping algorithm could still be utilized.

If we consider the thermodynamic driving force conjugate to ξ as proposed by Lagoudas et al.[12] which has the form

$$\begin{aligned} \pi = \boldsymbol{\sigma} : \boldsymbol{\Lambda} + \frac{1}{2}\boldsymbol{\sigma} : \Delta\mathcal{S} : \boldsymbol{\sigma} + \boldsymbol{\sigma} : \Delta\alpha\left(T - T_0\right) + \\ \rho\Delta c\left[\left(T - T_0\right) - Tln\left(\frac{T}{T_0}\right)\right] + \rho\Delta s_0 T - \rho\Delta u_0 - \frac{\partial f}{\partial \xi} \end{aligned} \tag{2.3}$$

then $\frac{\partial f}{\partial \xi}$ represents the hardening of the material and is unique for each of the options mentioned above. The new proposed "smooth" hardening function[20] takes the form

$$\frac{df}{d\xi} = \begin{cases} \frac{1}{2}a_1\left(1 + \xi^{n_1} - (1-\xi)^{n_2}\right); & \dot{\xi} > 0 \\ \frac{1}{2}a_2\left(1 + \xi^{n_3} - (1-\xi)^{n_4}\right); & \dot{\xi} < 0 \end{cases} \tag{2.4}$$

where constants a_1 and a_2 are again calibrated from the common SMA material parameters. However, n_1, n_2, n_3, and n_4 provide new descriptive parameters which are calibrated based on the smoothness of response in each of four transformation regions: beginning of forward, end of forward, end of reverse, and beginning of reverse, respectively. The effectiveness of this smooth form in capturing experimental response will be demonstrated in the following section.

3. EXPERIMENTAL CHARACTERIZATION AND MODEL CALIBRATION

To implement the model described above, particular parameters must be derived from experimental characterization. These parameters can be grouped into three catagories: thermoelastic properties, properties which describe conditions on transformation, and strain evolution properties. The needed parameters are listed here and methods of determination are briefly described:

The first subset of material parameters are the isotropic thermoelastic properties for the assumed isotropic polycrystalline SMA material.

- E^A, E^M: The elastic moduli of austenite and martensite, respectively. Determined during initial loading at high temperature before isobaric temperature sweeps were imposed and during SME testing, respectively.
- ν^A, ν^M: Poisson's Ratio of austenite and martensite, respectively. (Here taken from literature.)[12]
- α^A, α^M: The coefficient of thermal expansion of austenite and martensite, respectively. (Here taken from literature.)[12]

The next subset determines the locations of the transformation regions in the stress/temperature design space (i.e. when does a given transformation begin/end).

M_s, M_f, A_s, A_f: The zero-stress transformation temperatures found from the intersections of the transformation surfaces with the stress axis in the stress/temperature phase diagram.

$C^A|_\sigma, C^M|_\sigma$: Stress influence coefficients which describe the general slope of the transformation surfaces in the stress/temperature phase diagram. In this work, derived at a stress level of 300MPa and determined by the slopes of the transformation regions into austenite ($C^A|_{\sigma=300}$), and into martensite ($C^M|_{\sigma=300}$).

Finally, the remaining required parameters govern the evolution of ξ (i.e. via the hardening function) and represent the maximum transformation strain created as the material becomes fully martensitic.

$H^{cur}(\sigma)$: The maximum transformation strain generated during forward transformation as a function of stress. In this work, assumed to be an exponential function of efffective stress.

n_1–n_4: The smoothness parameters which govern the curvature at the beginning and end of each transformation.

The key set of experiments used to calibrate these various parameters are the constant load, variable temperature tests performed on tensile specimens. In this case, a single specimen was cut from the same raw material as the SMA beams and then stabilized (trained) by being cycled through 100 full transformations under a constant applied stress of 300 MPa. The trained specimen was then subjected to various lower stresses and full thermal cycles were applied. The transformation response of the specimens over the range of temperatures and at different applied stresses are shown in Fig. 1. The maximum transformation strains, $H^{cur}(\sigma)$, generated

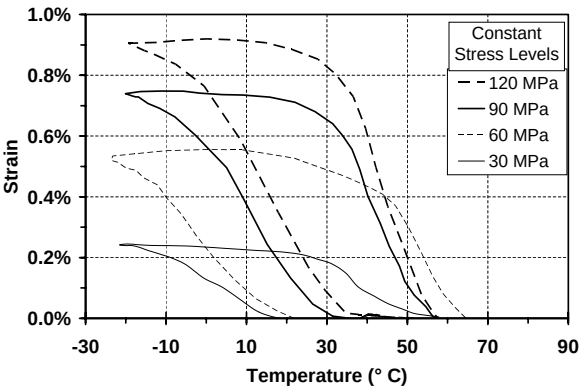

(a) Low applied constant stresses

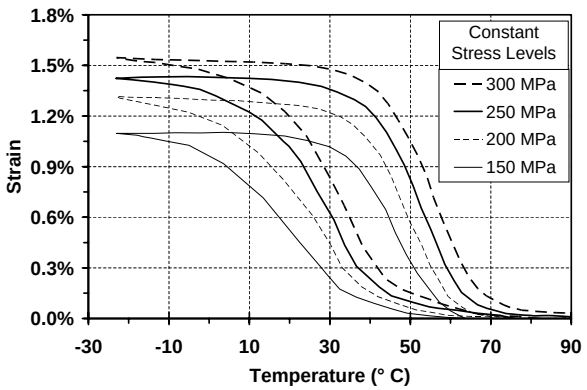

(b) Moderate and high applied constant stresses

Figure 1. Results of constant stress thermal cycling of Ni60Ti40 material.

by this trained specimen at each stress level are shown in Figure 2a. An exponential curve fit for the trained specimen has also been determined. The beginnings and endings of the phase transformations are also shown in stress/temperature space in Fig. 2b, including both the experimental data and appropriate analytical surfaces derived from the unified model and fit to this data. Based on these experiments, the values for all these parameters are given in Table 1. Note that the use of the smooth hardening function alters the required transformation start and finish temperatures, requiring M_s to be colder and A_f to be hotter than the extrapolated predictions made in Fig. 2b, for example.

Validation of both the model and the chosen material parameters then proceeded whereby the capability of the model to match the tensile test experimental results was assessed. A cube subjected to 1-D isobaric loading paths at three constant stresses (90, 150 MPa, and 200 MPa) was modeled using one set of material parameters (see Table 1), and the results were compared to experimental data. These results were shown above in the discussion of the hardening function (Fig. 3) and a very close agreement is observed. After this 1-D simulation of experimental results, the 3-D multi-component variable geometry chevron problem was modeled.

With the validation providing satisfactory results, calibration efforts were completed. The chosen parameters of Table 1 were used in all subsequent modeling. No re-calibrations were performed.

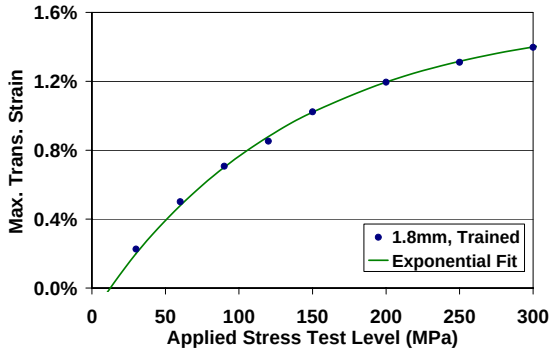

(a) Maximum transformation strain as a function of stress

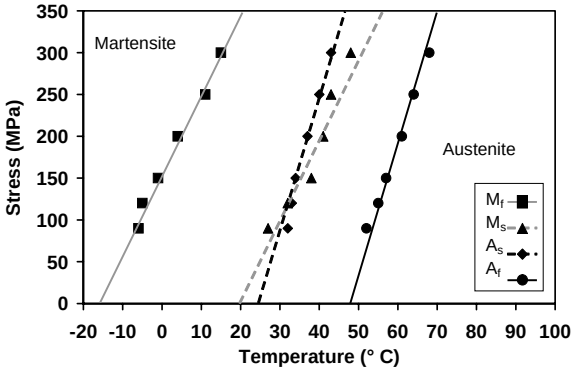

(b) Stress-temperature phase diagram

Figure 2. Reductions of constant stress thermal cycling data for calibration of the thermomechanical constitutive model.

Table 1. Unified model material parameters as defined for Ni60Ti, trained material.[15]

Parameter	Value
E^A	90GPA
E^M	63GPA
ν	0.33
$\alpha^M = \alpha^M$	10e-6/ °C
M_s	28 °C
M_f	−10 °C
A_s	27 °C
A_f	53 °C
$C^A\|_{\sigma=300MPa}$	15.9MPa/ °C
$C^M\|_{\sigma=300MPa}$	9.6MPa/ °C
$H^{cur}(\sigma)$	$= 0.0158[1 - \exp(-676.8\sigma/E^A)]$
η_1,η_2,η_3,η_4	0.6,0.2,0.2,0.3

4. VGC NUMERICAL ANALYSIS: RESULTS AND VALIDATION

Given the particular material model, the complimentary derived material properties, and the engineering design for the VGC system, it was then possible to begin numerical analysis of the full 3-D active structure. The prediction of the active Boeing VGC response to various thermal inputs provided a challenging boundary value problem which required powerful numerical tools. The previously mentioned FEA implementation of the unified model in an ABAQUS/Standard environment[15] was used to simulate this system. The system modeled consisted of multiple parts requiring careful consideration of their interfaces. The configuration of this assembly and the analysis results will be described below.

4.1. Model Preparation and Processing

The active Boeing VGC consists of a laminate substrate onto which three identical SMA pre-curved beams are attached. Over the majority of its surface the substrate itself consists of 15 layers, modeled using the ABAQUS `SHELL SECTION, COMPOSITE` command, and is assumed to be elastic. The fully three dimensional solid model is meshed with 6-node triangular shell (`STRI65`) elements and is assumed to be 3.16mm thick.

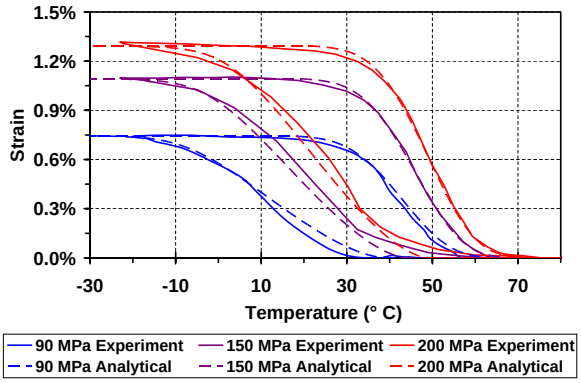

Figure 3. Simulation of experimental constant stress thermal cycling data using the calibrated constitutive model, including the smooth hardening function.

The active shape memory alloy components used on the Boeing VGC are varying cross-section, precurved shape memory alloy beams EDM cut from the center of a larger bulk plate (from which the tensile specimens characterized in Sect. 3 were also cut). For finite element modeling, 3-D solid models of such beams are meshed using quadratic "brick" elements with reduced integration (`C3D20R`), as such elements are noted by ABAQUS to be accurate in the modeling of bending. A total of 2100 elements were used to model each beam (70 along the length, five across the width, and six through the thickness). The constitutive behavior of each element was defined through the use of the aforementioned user material subroutine,[15] calibrated with the parameters derived via characterization and given in Table 1. This subroutine is called at each integration point during the solution process.

The proper assembly of these four total parts (one chevron substrate and three beams) involves several considerations. These include the manner in which the beams are forced flush with the substrate and held there ("clamping"), how non-penetration or contact is enforced at the beam/substrate interface, and what methods are used to prevent unreasonable beam rotations. Relative downward motion of the beams toward the substrate was enforced using ABAQUS `SLOT` connector elements which can prescribe collinear motion along a single axis. In this case the clamping axis was aligned with that of the bolts as installed on the flight tested chevron.[10] Unreasonable penetration of the SMA beams through the chevron substrate was prevented by defining contact regions on the ends of each beam with matching regions being defined over a small local subset of the adjacent chevron surface. Using ABAQUS internal contact algorithms, this enforced that the beam tips could only slide tangent to the chevron while the normal contact forces caused bending of the chevron. Note that frictionless sliding contact was assumed in this analysis which is compatible with the fabrication of the chevron prototypes which incorporated lubrication at the interface. Finally, unreasonable beam rotations about the bolt axis were prevented by the use of `SLIDE-PLANE` connector elements which enforced that the beam tips only deform in a plane containing the beam longitudinal axis (in the reference configuration) and the bolt axis. The fully assembled 3-D FEA model is shown below in Figure 4, with the connector elements being schematically illustrated. Both isometric and side views are shown.

4.2. Multi-component and Subcomponent Preliminary Analysis and Validation

Before validating the ability of the analysis tools to predict the actuation behaviour of the complete chevron assembly experiencing specified thermal inputs, preliminary experiments and related analyses were first performed. Two particular analysis types were performed: *i.* point loading at the tip of the chevron (SMA beams installed, no phase transformation) and *ii.* thermal cycling of the active SMA beam under applied load. Such tests were performed both experimentally at the Boeing facilities and numerically at TAMU. The results of each of these analysis are given below.

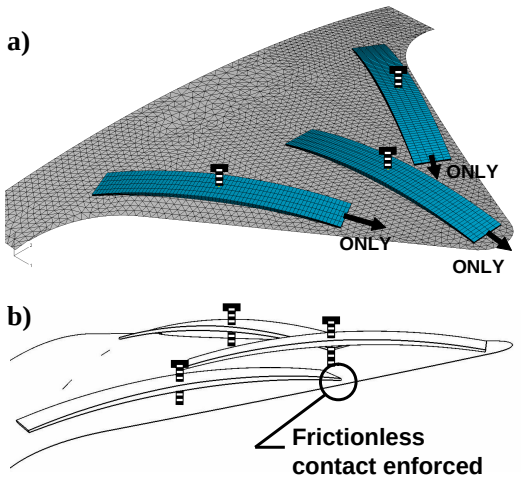

Figure 4. Assembled 3-D FEA model of the VGC system in isometric view (a) and side view, highlighting precurvature of SMA beams (b). Note that clamping connector elements are shown schematically.

4.2.1. Elastic multi-component response

The initial set of preliminary analyses validated the ability to accurately model the elastic response of the total chevron system. To this end, all three SMA beams were transformed fully into martensite and then were installed on the chevron. A point load of 227N downward (into the fan flow) was then applied at the chevron tip. In the experimental setup, photogrammetry was used to determine the surface topography of the chevron under different loading conditions. In this process, multiple cameras are used to stereographically determine the 3-D location of various reflective "dots" or targets applied to the substrate surface. The topological contours for the analytical case are derived by summing the reference locations with the displacements for each node in the mesh. The surface topography contours which resulted from this elastic loading case (experimental and analytical) are shown in Fig. 5.

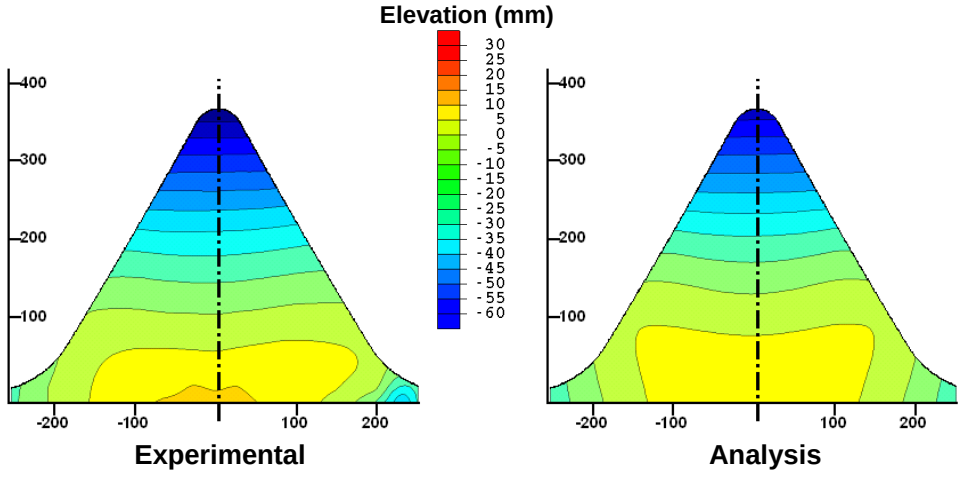

Figure 5. Comparison of results for -227N tip loading of chevron substrate with martensitic beams installed - experimental and FEA model.

4.2.2. Active SMA beam response

The ability of the implemented model to accurately capture the transformation behavior of a monolithic 3-D structural element was ascertained by modeling of the tapered, precurved active SMA beam subject to thermomechanical loading.

The SMA beam validation problem was as follows: the two ends of the precurved beam were placed in contact with a flat, rigid, frictionless plane while the center of the beam, initially in equilibrium above this plane, was forced downward toward the plane with some force (constant or linearly varying with deflection). In the analysis, this was performed by applying appropriate boundary conditions to the beam mesh while a concentrated load was applied at the center node of the beam and quasistatic thermal cycles were also applied. The boundary conditions implied constrained the beam tips in the direction normal to the rigid plane. Experimentally, the SMA beam was placed on a rigid brass plane mounted on an MTS loading frame. Lubrication was used at the beam/plane interface. The load was applied to the center of the beam by the MTS and was measured by a load cell. Deflection was logged by monitoring crosshead displacement. For changing beam temperature, this entire setup was placed within a heating/cooling chamber. This experimental setup can be seen (without thermal chamber) in Fig. 6a.

Two kinds of loading were applied to the center of the beam. The first considered a 90 N constant load while the second considered a load which decreased linearly as the beam deflection increased (from curved toward flat). The spring rate for this variable load was 63 N/mm. The experimental and analytical deflection vs. temperature results are shown in Fig. 6b. Note that both results show general agreement, but that the modeling predictions for the spring biasing force are more accurate. This is because the stress levels present in the beam during the variable force loading (up to 160 MPa) are much higher than for the constant 90 N loading (up to 40 MPa), thereby incorporating calibration data from a greater number of constant stress calibration tests. Such variable loading is also a better simulation of loading conditions experienced by the beam when incorporated into the actual chevron system.

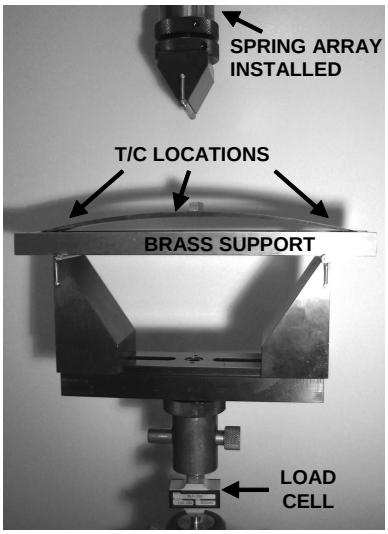

(a) Experimental setup (side view)

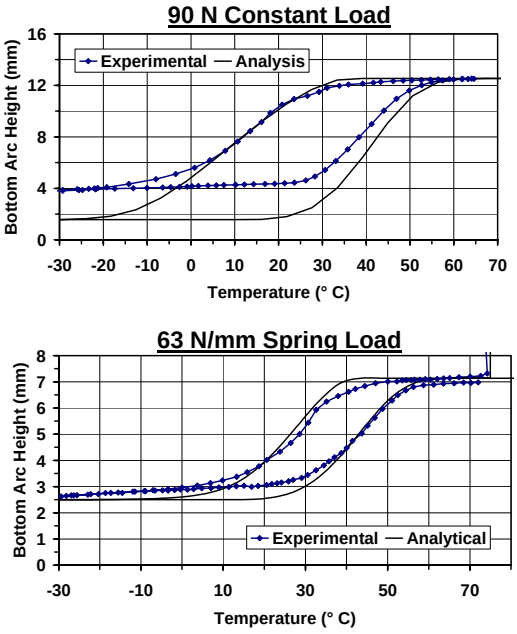

(b) Experimental and analytical results

Figure 6. Setup and results for experimental validation of thermomechanical SMA beam modeling.

4.3. Active Multi-component VCG Final Validation

The most rigorous validation of the model accuracy as implemented in this FEA framework was performed by considering the overall VGC response to thermal inputs. The same assembly of elastic composite substrate with three SMA beams (described previously) was again modeled. In this case, four thermomechanical loading steps were applied to this multi-component chevron system. These included one step to test/model system assembly (Step 1) and an additional three steps to test/model a full cycle of system actuation. The loading steps applied to both the experimental prototype and FEA model were as follows:

1. Clamp the beams in the martensitic state onto the substrate until fully flush.
2. Heat the beams through full transformation into austenite.
3. Cool the beams to room temperature (20°C) during which transformation into martensite is initiated but *not* completed.
4. Heat the beams through full transformation into austenite once again.

The surface topography of the reference configuration, at the end of the cooling step, and at the end of the final heating step are shown via the contour plots provided in Fig. 7. Note that the reference configuration is the stress-free configuration with no SMA beams attached and no loads applied. Both experimental and numerical results are shown, and the numerical predictions are noticeably accurate. In examining the predictions for $T = 80\,^{\circ}\mathrm{C}$, it was calculated that the least-squares error over all measured points along the centerline in particular was $\sim 6\%$

5. CONCLUSIONS

It has been shown in this work that accurate thermomechanical response predictions of smart structures incorporating active materials (i.e., shape memory alloys) can be calculated by current phenomenological models as calibrated by careful, standardized experimentation. The numerical analysis tool chosen was an SMA phenomenological model which was modified to include effects important for the specific material system of choice (Ni60Ti). The experimentation required was shown to be straightforward in that only isothermal and/or constant stress tests were sufficient to fully and accurately calibrate the constitutive model. The FEA implementation of the model was used to analyze a smart structure, specifically a variable geometry jet engine chevron composed of an elastic composite substrate onto which active SMA beams are installed. The predictions of the FEA for subcomponents and for the multi-component VGC structure were compared directly to experimental results. The predictions for the total VGC had an error of much less than 10%.

This ability to model multi-component smart structures including contact is important as engineers and designers in more industrial sectors continue to discover the benefits of SMA utilization as an enabling technology. By incorporating these tools, the legacy method of arriving at final smart structure designs based solely on design-build-test cycles can be augmented and analytical results used to both expedite and improve the overall design process.

ACKNOWLEDGMENTS

The authors would like to acknowledge the financial support of the National Defense Science and Engineering Grant (NDSEG) and the NSF Integrative Graduate Education and Research Traineeship (NSF-IGERT) which funded D. Hartl over the course of this work. Our thanks is also extended to the staff of the Material Structures Laboratory at Texas A&M University, specifically Rodney Inmon, for his constant help in all experimental efforts.

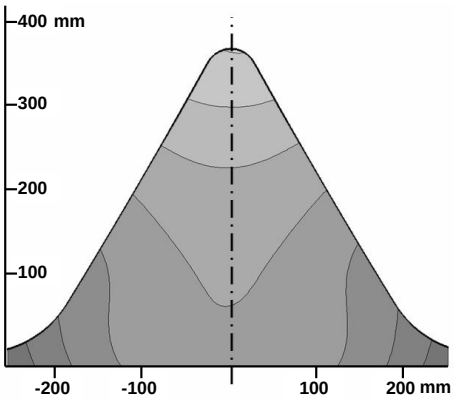

(a) Reference (analysis)

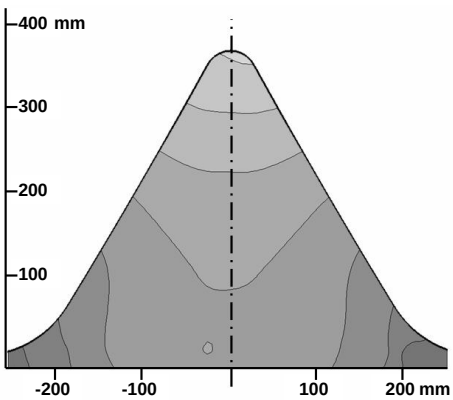

(b) Reference (experimental)

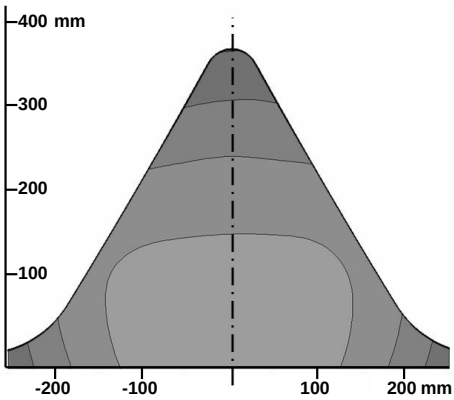

(c) Heated, $T = 80\,^{\circ}\mathrm{C}$ (analysis)

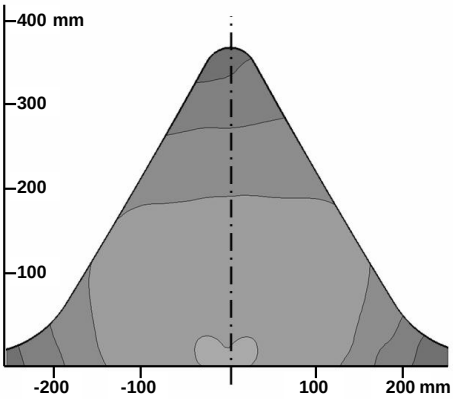

(d) Heated, $T = 80\,^{\circ}\mathrm{C}$ (experimental)

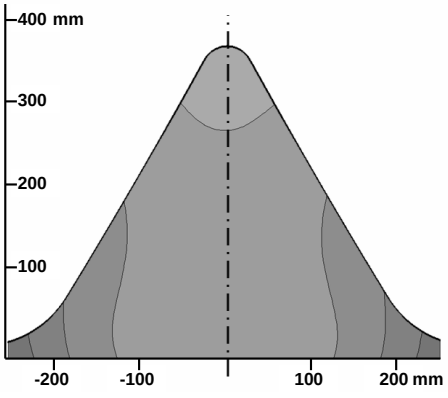

(e) Cooled, $T = 20\,^{\circ}\mathrm{C}$ (analysis)

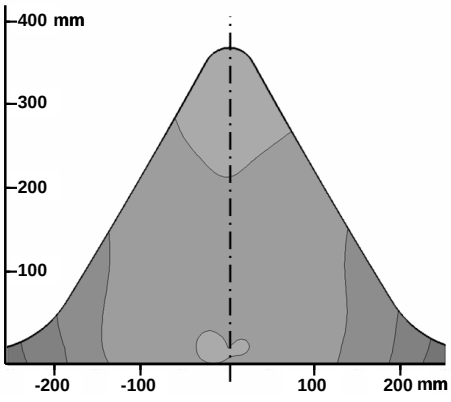

(f) Cooled, $T = 20\,^{\circ}\mathrm{C}$ (experimental)

Figure 7. Topography of the VGC: reference state, heated SMA beams, and cooled SMA beams.

REFERENCES

1. D. J. Hartl and D. Lagoudas, "Aerospace applications of shape memory alloys," *Proceedings of the Institution of Mechanical Engineers, Part G: Journal of Aerospace Engineering* **221 (Special Issue)**, pp. 535–552, 2007.
2. K. R. Melton, "General applications of shape memory alloys and smart materials," in *Shape Memory Materials*, K. Otsuka and C. M. Wayman, eds., ch. 10, pp. 220–239, Cambridge University Press, Cambridge, 1999.
3. J. Kudva, "Overview of the DARPA smart wing project," *Journal of Intelligent Material Systems and Structures* **15**, pp. 261–267, 2004.
4. P. Jardine, J. Flanigan, and C. Martin, "Smart wing shape memory alloy actuator design and performance," in *Proceedings of SPIE, Smart Structures and Materials*, **3044**, pp. 48–55, (San Diego, CA), March 3–6 1997.
5. D. Pitt, J. Dunne, E. White, and E. Garcia, "SAMPSON smart inlet SMA powered adaptive lip design and static test," *Proceedings of the 42nd AIAA Structures, Structrual Dynamics, and Materials Conference, Seattle, WA, 16–20 April 2001* , pp. 1–11, 2001.
6. J. K. Strelec, D. C. Lagoudas, M. A. Khan, and J. Yen, "Design and implementation of a shape memory alloy actuated reconfigurable wing," *Journal of Intelligent Material Systems and Structures* **14**, pp. 257–273, 2003.
7. K. Singh and I. Chopra, "Design of an imporoved shape memory alloy actuator for rotor blade tracking," in *Proceedings of SPIE, Smart Structures and Materials*, *Proceedings of SPIE, Smart Structures and Materials, San Diego, CA, 17–21 March 2002* **4701**, pp. 244–266, (San Diego, CA), 17–21 March 2002.
8. N. Caldwell, A. Glaser, E. Gutmark, and R. Ruggeri, "Heat transfer model for blade twist actuator system," in *Proceedings of 44th AIAA Aerospace Sciences Meeting and Exhibit*, pp. 1–22, 9–12 January 2006.
9. F. Calkins, G. Butler, and J. Mabe, "Variable geometry chevrons for jet noise reduction," *Proceedings of the 27th Annual AIAA Aeroacoustics Conference* , pp. 1–11, 8–10 May 2006.
10. J. H. Mabe, F. Calkins, and G. Butler, "Boeing's variable geometry chevron, morphing aerostructure for jet noise reduction," in *47th AIAA/ ASME / ASCE / AHS / ASC Structures, Structural Dynamics and Materials Conference*, pp. 1–19, (Newport, Rhode Island), 1–4 May 2006.
11. T. Turner, R. Buehrle, R. Cano, and G. Fleming, "Modeling, fabrication, and testing of a SMA hybrid composite jet engine chevron concept," *Journal of Intelligent Material Systems and Structures* **17**, pp. 483–497, June 2006.
12. D. C. Lagoudas, Z. Bo, and M. A. Qidwai, "A unified thermodynamic constitutive model for SMA and finite element analysis of active metal matrix composites," *Mechanics of Composite Materials and Structures* **3**, pp. 153–179, 1996.
13. M. A. Qidwai and D. C. Lagoudas, "Numerical implementation of a shape memory alloy thermomechanical constitutive model using return mapping algorithms," *International Journal for Numerical Methods in Engineering* **47**, pp. 1123–1168, 2000.
14. D. Lagoudas, ed., *Shape Memory Alloys: Modeling and Engineering Applications*, Springer-Verlag, 2008.
15. D. Lagoudas, Z. Bo, M. Qidwai, and P. Entchev, *SMA_UM: User Material Subroutine for Thermomechanical Constitutive Model of Shape Memory Alloys.* Texas A&M University, College Station, TX, March 2003.
16. Z. Bo and D. C. Lagoudas, "Thermomechanical modeling of polycrystalline SMAs under cyclic loading, Part I: Theoretical Derivations," *International Journal of Engineering Science* **37**, pp. 1089–1140, 1999.
17. K. Tanaka, S. Kobayashi, and Y. Sato, "Thermomechanics of transformation pseudoelasticity and shape memory effect in alloys," *International Journal of Plasticity* **2**, pp. 59–72, 1986.
18. J. G. Boyd and D. C. Lagoudas, "A thermodynamical constitutive model for shape memory materials. Part I. The monolithic shape memory alloy," *International Journal of Plasticity* **12**(6), pp. 805–842, 1996.
19. C. Liang and C. A. Rogers, "One-dimensional thermomechanical constitutive relations for shape memory materials," *Journal of Intelligent Material Systems and Structures* **1**, pp. 207–234, 1990.
20. L. Machado, D. Lagoudas, and M. Savi, "Lyapunov exponents estimation for hysteretic systems." submitted, 2007.